POLITECNICO DI TORINO
Repository ISTITUZIONALE

Pseudorange and Doppler-Based State Estimation from MEO to LEO: A Comprehensive Analysis of Maximum Likelihood Estimators

(Article begins on next page)

28 April 2024

Pseudorange and Doppler-based State Estimation from MEO to LEO: A Comprehensive Analysis of Maximum Likelihood Estimators

Luca Morichi (iD), Alex Minetto (iD), Andrea Nardin (iD), Simone Zocca (iD), Fabio Dovis (iD), *Politecnico di Torino, Turin, Italy*

BIOGRAPHY

Luca Morichi received a B.Sc. in Telecommunication Engineering in 2022 and a M.Sc. in Communication and Computer Networks Engineering in 2023, both from Politecnico di Torino (Turin, Italy). He is currently a Ph.D. student within the Navigation Signal Analysis and Simulation (NavSAS) group at Politecnico di Torino. His research is focused on the design and optimization of radionavigation signals and modulations for modernized MEO and LEO PNT services.

Alex Minetto received the B.Sc., and M.sc. degrees in Telecommunications Engineering from Politecnico di Torino, Turin, Italy and his Ph.D. degree in Electrical, Electronics and Communications Engineering, in 2020. He joined the Department of Electronics and Telecommunications of Politecnico di Torino in 2021 as researcher and assistant professor. His current research interests cover navigation signal design and processing, advanced Bayesian estimation applied to Positioning and Navigation Technologies (PNT) and applied Global Navigation Satellite System (GNSS) to space weather and space PNT.

Andrea Nardin received the M.Sc. degree in Telecommunications engineering and the Ph.D. degree in Electrical, Electronics and Communications Engineering, in 2018 and 2023, respectively, both from Politecnico di Torino, where he is currently a postdoctoral researcher. From 2018, he has been working on satellite navigation technologies with the Navigation Signal Analysis and Simulation (NavSAS) group at Politecnico di Torino and in 2021 he was a Visiting Doctoral Researcher at Northeastern University, Boston, MA, USA with the Information Processing Lab (IPL).

Simone Zocca received a B.Sc. in Telecommunication Engineering in 2018 and a M.Sc. in Communication and Computer Networks Engineering in 2020, both from Politecnico di Torino (Turin, Italy). He is currently a Ph.D. student within the Navigation Signal Analysis and Simulation (NavSAS) group at Politecnico di Torino. His research is focused on innovative solutions for signal processing techniques and Bayesian estimation applied to Global Navigation Satellite System (GNSS).

Fabio Dovis received his M.Sc. degree in 1996 and his Ph.D. degree in 2000, both from Politecnico di Torino, Turin, Italy. He joined the Department of Electronics and Telecommunications of Politecnico di Torino as an assistant professor in 2004 and as associate professor in 2014. Since 2021 he is a full professor. He coordinates the Navigation Signal Analysis and Simulation (NavSAS) research group. His research interests cover the design of GPS and Galileo receivers, advanced signal processing for interference and multipath detection and mitigation, as well as ionospheric monitoring.

ABSTRACT

Recent research into state estimation algorithms for Low Earth Orbit (LEO) satellites, driven in part by the emergence of broadband LEO constellations, has stimulated interest in their application to Position, Navigation and Timing (PNT). This study investigates the effectiveness of Doppler measurements as a complementary solution for positioning and compares them with conventional pseudorange-based methods in Global Navigation Satellite Systems (GNSSs). The study highlights a limitation in Maximum Likelihood (ML) estimators, especially Least Squares (LS), which affect the convergence of positioning algorithms, especially when dealing with satellites in the LEO region. To analyse this problem, we developed a theoretical framework called "satellite scale-down". We then used Monte Carlo simulations to investigate the relationship between the initialisation point of the algorithm and orbital altitude. We also examined the algorithm's performance with satellites positioned at different orbital altitudes. The results indicate that decreasing the orbital radius enhances the performance of the Doppler-based positioning algorithm; however, it makes the LS positioning algorithm more sensitive to the initialisation point. In fact, without any a priori data on the receiver, the algorithm fails to converge. Therefore, it is necessary to make a trade-off between the achievable performance and the available information about the receiver.

I. INTRODUCTION

In recent years, there has been a noteworthy interest in investigating state estimation algorithms to determine a user's Position Velocity and Time (PVT) through Low Earth Orbit (LEO) satellites. This growing interest is mainly due to the emergence of broadband LEO constellations providing global communication services (Reid et al., 2018; Kassas, 2021; Kozhaya and

Kassas, 2023). The interest in exploiting new constellations in the LEO region, such as Iridium, OneWeb, and Starlink, stems from the need to overcome the inherent limitations of Global Navigation Satellite System (GNSS) in the Medium Earth Orbit (MEO) region. These limitations include signal degradation, extensively documented in the literature, especially in complex environments such as urban canyons, areas with dense vegetation, or indoor environments. Furthermore, it is essential to consider the presence of interference, whether intentional, with the risk of signal loss, or deliberate, as in the case of jamming attacks aimed at compromising the service. In this respect, LEO satellites can provide higher signal power due to their proximity to the Earth (Reid et al., 2018; Khalife and Kassas, 2019). An increase of about 30 dB is estimated compared to the traditional GNSS system based on MEO satellites (Khalife and Kassas, 2019).

However, employing LEO satellites brings its own set of challenges. One major obstacle is the limited coverage provided by the footprint of LEO satellites, which is considerably smaller than that of MEO. Consequently, achieving global coverage comparable to GNSSs requires a more extensive satellite constellation. To meet this challenge, there is the option of using satellites mega-constellations in the LEO region designed for Internet connectivity, provided the cost is worth it. It is crucial to note, however, that these satellites are not intended for navigation services. They lack essential features such as accurate timing, and their signals are neither designed nor optimised for ranging (Psiaki, 2021). Therefore, a positioning technique based on a Frequency Division Multiple Access (Frequency-division multiple access (FDMA)) approach, utilising only Doppler shift, akin to the one employed in the Transit system in the early days of satellite navigation, is being reconsidered. Implementing this technique in the LEO region offers the advantage of exploiting a greater variability in Doppler measurements due to the speed of the satellites (Reid et al., 2018; Shi et al., 2023). Furthermore, the transmission of solely the navigation message results in a bandwidth advantage, eliminating the necessity of transmitting the spreading code (Van Graas, 2023).

A wide range of scientific contributions is investigating the efficacy of Doppler measurements as either a standalone or complementary source of positioning data, with the potential to replace or supplement conventional pseudorange-based solutions commonly adopted in GNSSs.

In (Psiaki, 2021) the authors proposes a navigation method based solely on Doppler measurement. His algorithm aims to estimate eight state uknowns: position in 3D, clock bias, speed in 3D and clock drift. This algorithm was tested using the Starlink constellation, which includes 2825 satellites, and produced promising results. In addition, the author presents an analysis of Geometric Dilution of Precision (GDOP) by introducing scaling factors, which was tested using both the OneWeb and Starlink constellations.

Also in (Shi et al., 2023), a navigation method based only on Doppler measurement is proposed. In this case, the algorithm is designed to resolve seven state uknowns: position in 3D, speed in 3D and clock drift. The paper presents an error analysis, taking into account inaccurate satellite positions and velocities, as well as delays introduced by the ionosphere and troposphere. It is important to note that in LEO orbit, these delays have a greater impact than in MEO orbit, due to the high velocities of the satellites. Finally, the article tests the convergence of the algorithm for different initial configurations.

Authors in (Tan et al., 2019) investigate Doppler-based positioning using signals from the IRIDIUM constellation, treated as Signal of Opportunitys (SOPs). In addition, they analyse the orbital errors of satellites by developing a new geometric method based on the positioning surface, which, in Doppler-based positioning, has a conical shape.

In (Van Graas, 2023), several techniques for Doppler processing are summarised. The authors not only present a positioning algorithm based on Doppler measurements but also introduce the complementary Doppler filter, which proves useful for several purposes. This filter helps to increase the effective track duration to improve accuracy, allows the use of continuous Doppler signals from satellites with a shorter integration time than the track duration, maintains a position solution when fewer satellites are available (such as less than seven when time is known or less than eight when time is unknown), and increases the update rate of position, velocity and clock offset solutions. Furthermore, the authors tested the effectiveness of this algorithm on flight test data, the results of which demonstrate excellent accuracy at metre level due to the application of the complementary Doppler filter.

To the best of the authors' knowledge, much of the literature on Doppler positioning does not initialise the iterative positioning algorithm based on the Least Square (LS) estimator at the centre of the Earth, as is commonly done. This approach requires some prior knowledge of the receiver position. Only (Shi et al., 2023) explicitly considers the algorithm's responsiveness to the initiation point. In this paper, our objective is to begin a more general investigation of the Doppler-based positioning algorithm, to extend its applicability. The study begins by examining the performance of the Doppler-based positioning algorithm with GPS satellites in MEO and compares it with the code-based approach. Subsequently, the investigation delves into theoretical scenarios that entail positioning satellites at varying orbital altitudes, especially at lower altitudes than those of the GPS, and analyses the impact on system performance. Additionally, in these situations, the performance analysis is complemented by an evaluation of the algorithm's convergence as the altitude of the satellite orbit varies.

The remainder of this paper is as follows. In Section II we provide a basic overview of the fundamentals behind the LS algorithm based both Doppler and Pseudorange measurements. In Section III, we outline the theoretical framework of "satellite

scale-down", which is then applied in section IV. Here we present the results of our investigation, focusing on the analysis of a static receiver. First, we examine the performance by using the GPS system satellites in their original positions. Next, we integrate this scenario into the theoretical framework of "satellite scale-down", exploring the implications when the orbital radius of the satellite decreases. Finally in section V we drew the conclusions of our work.

II. BACKGROUND

GNSS-based services are concerned with solving the so-called PVT problem, aiming to determine the homonym information about the receiver. These information, estimated through the positioning problem, constitutes what is commonly referred to as the receiver state. A generic state can be defined as:

$$\mathbf{x} = \begin{bmatrix} \mathbf{r}_u \\ \mathbf{v}_u \\ \boldsymbol{\tau}_u \end{bmatrix} \tag{1}$$

where $\mathbf{r}_u$ represents a 3-component vector denoting the user's position with respect to a specific reference frame, $\mathbf{v}_u$ stands for a 3-component vector representing the user's speed, and $\boldsymbol{\tau}_u$ is a generic vector containing unknown local clock offset and drift with respect to a given time scale. To estimate the terms in (1), the receiver relies on the observables and related measurements derived from signals received from satellites. For example, the GNSS standard, is based on the signal travelling time observable, from which pseudorange measurements can be constructed as follows:

$$\rho_i = \|\mathbf{r}_i - \mathbf{r}_u\| + c\delta t_u + \epsilon_{\rho_i} \tag{2}$$

where ρ_i denotes the pseudorange measurements associated with the i-th satellite, and $c\delta t_u$ represents the satellite clock bias, a parameter that accounts for the time offset between the user and the GNSS time scale. ϵ_{ρ_i} characterises the noise in the pseudorange measurements for the i-th satellite.

An alternative to this approach, is to leverage the Doppler shift observable and pseudorange rate measurement. The Doppler shift impacts the frequency received by the GNSS receiver, primarily due to the relative motion between the receiver and the satellite. This shift leads to a variation in the received frequency (f_{RX}) concerning the transmitted one (f_{TX}), it can be described as (Braasch and van Dierendonck, 1999):

$$f_{D_i} = f_{RX} - f_{TX} = -v_{D_i} \lambda_{TX}^{-1} \tag{3}$$

where f_{D_i} represents the Doppler frequency shift for the i-th satellite, expressed in Hertz (Hz). v_{D_i} denotes the radial component of the relative velocity between the satellite and the user, i.e., $\mathbf{v}_{r_i}$, which can be defined as the difference between the velocity vector of the i-th satellite ($\mathbf{v}_i$) and the user's velocity vector ($\mathbf{v}_u$). Additionally λ_{TX} represents the wavelength of the transmitted signal.

The radial velocity v_{D_i}, defined as the projection of the relative velocity along the Line of Sight (LOS) between the satellite and the receiver, is also referred to as range rate and is modelled mathematically with the following dot product equation:

$$v_{D_i} = \|\underbrace{\mathbf{v}_i - \mathbf{v}_u}_{\mathbf{v}_{r_i}}\| \cdot \frac{\mathbf{r}_i - \mathbf{r}_u}{\|\mathbf{r}_i - \mathbf{r}_u\|} \tag{4}$$

Equation (3) is an approximation of the Doppler shift, which only considers the first order term of the true equation, omitting higher order terms (Bahrami and Ziebart, 2010). However, this approximation holds true when the relative velocity is significantly smaller than the speed of light (c).

The measurement associated to the Doppler shift observable is the pseudorange rate, that for the i-th satellite can be written as:

$$\dot{\rho}_i = (\mathbf{v}_i - \mathbf{v}_u) \cdot \frac{\mathbf{r}_i - \mathbf{r}_u}{\|\mathbf{r}_i - \mathbf{r}_u\|} + c\delta\dot{t}_u + \epsilon_{\dot{\rho}_i} \tag{5}$$

where the term $\delta\dot{t}u$ represents the drift of the user clock and indicates whether the clock is fast or slow with respect to the GNSS system time. Note that convention dictates that the sign of the clock drift is positive if the clock is running faster and negative if it is running slower, $\epsilon_{\dot{\rho}_i}$ represents the i-th pseudorange rate measurement noise.

The measurements described by (2) and (5) can be interpreted geometrically. In particular, equation (2), which characterises a pseudorange, i.e., a distance, can be visualised as the radius of a sphere centred on the satellite. The surface of the sphere characterise the locus of the points at the distance of the pseudorange from the satellite, as shown in Figure 1a. The pseudorange rate equation (5), on the other hand, can be interpreted as a circular conical surface (Tan et al., 2019). Specifically, all potential user positions with the same Doppler measurement collectively define a cone in the plane. The vertex of this cone corresponds to the satellite's position, while the axis aligns with the cone's relative velocity. Figure 1b provides a visual representation of the conical surface. Further insights into the geometry of Doppler positioning and its implications are detailed in (Tan et al., 2019).
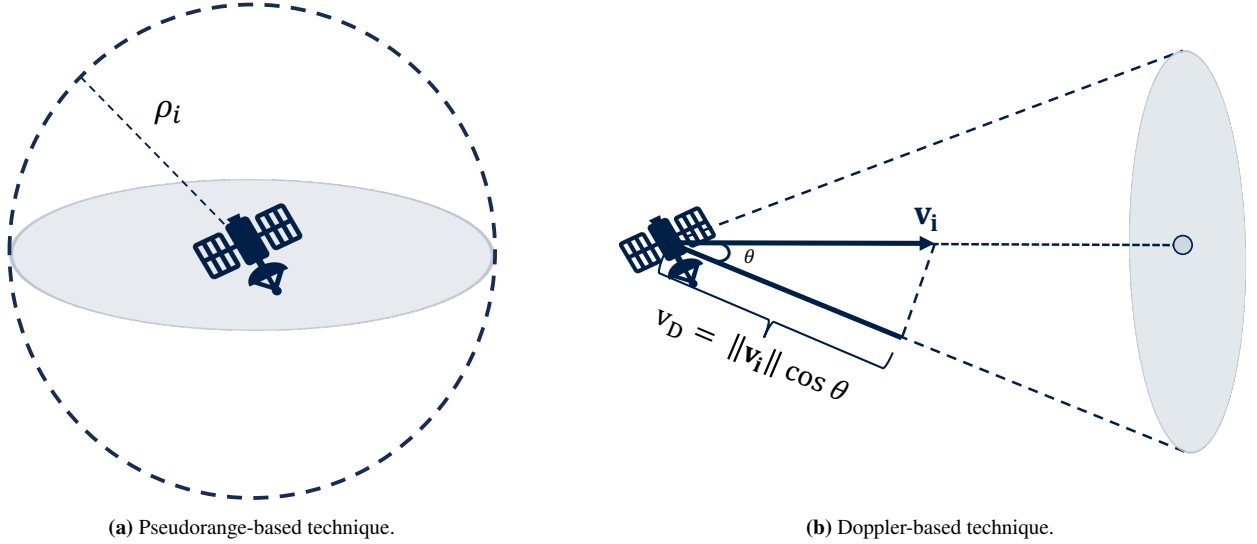

(a) Pseudorange-based technique.

(b) Doppler-based technique.

Figure 1: Positioning surfaces.

From the measurement equations, we can identify the elements of the receiver state that we want to estimate. As for the pseudorange equation (2), the positioning problem is based on the estimation of $n = 4$ unknowns, 3 to identify the user's position and one for the clock bias. On the other hand, for the pseudorange rate (5), if no prior information on the receiver state is available, the PVT problem involves dealing with $n = 7$ unknowns. Of these, 3 define the position of the receiver, 3 define its velocity and 1 takes into account the clock drift. If we have more information about the receiver, the number of unknowns can be reduced. For example, if the receiver is static, it can be shown that the 3 velocity components can be neglected.

Regardless of the measurement one chooses for positioning, the state estimate can be found by applying an iterative algorithm based on the LS estimator. In each iteration, before applying the LS estimator, the problem is linearised using the estimate generated in the previous iteration. Consequently, the solution in each iteration is of the type:

$$\mathbf{\Delta x} = (\mathbf{H}^T \, \mathbf{H})^{-1} \, \mathbf{H}^T \, \mathbf{\Delta f} \tag{6}$$

where, $\mathbf{\Delta x}$ is a vector with n components, representing the displacements between the true and estimated state parameters. Similarly, $\mathbf{\Delta f}$ is an m-component vector, capturing the displacements between the true measurement and the one computed at the linearization point. The variable $\mathbf{f}$ denotes a generic measurement, which in this case, based on what we have discussed earlier, can take the form of either a pseudorange measurement, yielding $\Delta\rho$, or a pseudorange rate measurement, resulting in $\Delta\dot{\rho}$. The Jacobian matrix $\mathbf{H}$ is an $m \times n$ matrix that establishes the relationship between the measurements and the state.

Equation (6) is in general form and applicable to both the measurements under analysis. In the following, we will use a subscript to specify which of the two measurements is considered. Specifically, for the pseudorange measurement we will use $(\cdot)_P$ subscript and for the pseudorange rate measurement we will use $(\cdot)_D$ subscript.

The Jacobian matrix is derived directly from (2) and (5), by taking the partial derivatives with respect to the elements of the state vector that for (2) can be written as $\mathbf{x_P} = [x \; y \; z \; c\delta t_u]^T$, while for (5) can be written as: $\mathbf{x_D} = [x \; y \; z \; v_{xu} \; v_{yu} \; v_{zu} \; c\dot{\delta t_u}]^T$.

The first three components of both $\mathbf{x_P}$ and $\mathbf{x_D}$, corresponds to user position, the resulting expression, as also noted in (Grewal et al., 2001; Lethinen, 2002), takes the form:

$$\frac{\partial \rho_i}{\partial \mathbf{r}_u} = \left\{ \frac{\mathbf{r}_u - \mathbf{r}_i}{\|\mathbf{r}_i - \mathbf{r}_u\|} \right\}^T \tag{7}$$

$$\frac{\partial \dot{\rho}_i}{\partial \mathbf{r}_u} = \left\{ \frac{\mathbf{r}_i - \mathbf{r}_u}{\|\mathbf{r}_i - \mathbf{r}_u\|} \times \left(\frac{\mathbf{r}_i - \mathbf{r}_u}{\|\mathbf{r}_i - \mathbf{r}_u\|} \times \frac{\mathbf{v_i}}{\|\mathbf{r}_i - \mathbf{r}_u\|} \right) \right\}^T \tag{8}$$

When we derive (5) with respect to the second set of three components in $\mathbf{x_D}$, which represents the user's speed, we obtain:

$$\frac{\partial \dot{\rho}_i}{\partial \mathbf{v}_u} = \left\{ \frac{\mathbf{r}_i - \mathbf{r}_u}{\|\mathbf{r}_i - \mathbf{r}_u\|} \right\}^T \tag{9}$$

Finally, analysing (2) can be easily find that $\frac{\partial \rho_i}{\partial \mathbf{c}\delta \mathbf{t_u}} = 1$ and similarly for (5) we have: $\frac{\partial \dot{\rho}_i}{\partial \mathbf{c}\delta \mathbf{t}_u} = 1$. Consequently, we obtain the following expressions for Jacobian matrices:

$$\mathbf{H}_P = \begin{bmatrix} \left\{ \frac{\mathbf{r}_1 - \mathbf{r}_u}{\|\mathbf{r}_1 - \mathbf{r}_u\|} \right\}^T & 1 \\ \left\{ \frac{\mathbf{r}_2 - \mathbf{r}_u}{\|\mathbf{r}_2 - \mathbf{r}_u\|} \right\}^T & 1 \\ \vdots & \vdots \\ \left\{ \frac{\mathbf{r}_m - \mathbf{r}_u}{\|\mathbf{r}_m - \mathbf{r}_u\|} \right\}^T & 1 \end{bmatrix} \tag{10}$$

$$\mathbf{H}_D = \begin{bmatrix} \left\{ \frac{\mathbf{r}_1 - \mathbf{r}_u}{\|\mathbf{r}_1 - \mathbf{r}_u\|} \times \left(\frac{\mathbf{r}_1 - \mathbf{r}_u}{\|\mathbf{r}_1 - \mathbf{r}_u\|} \times \frac{\mathbf{v_1}}{\|\mathbf{r}_1 - \mathbf{r}_u\|} \right) \right\}^T & \left\{ \frac{\mathbf{r}_1 - \mathbf{r}_u}{\|\mathbf{r}_1 - \mathbf{r}_u\|} \right\}^T & 1 \\ \left\{ \frac{\mathbf{r}_2 - \mathbf{r}_u}{\|\mathbf{r}_2 - \mathbf{r}_u\|} \times \left(\frac{\mathbf{r}_2 - \mathbf{r}_u}{\|\mathbf{r}_2 - \mathbf{r}_u\|} \times \frac{\mathbf{v_2}}{\|\mathbf{r}_2 - \mathbf{r}_u\|} \right) \right\}^T & \left\{ \frac{\mathbf{r}_2 - \mathbf{r}_u}{\|\mathbf{r}_2 - \mathbf{r}_u\|} \right\}^T & 1 \\ \vdots & \vdots & \vdots \\ \left\{ \frac{\mathbf{r}_m - \mathbf{r}_u}{\|\mathbf{r}_m - \mathbf{r}_u\|} \times \left(\frac{\mathbf{r}_m - \mathbf{r}_u}{\|\mathbf{r}_m - \mathbf{r}_u\|} \times \frac{\mathbf{v_m}}{\|\mathbf{r}_m - \mathbf{r}_u\|} \right) \right\}^T & \left\{ \frac{\mathbf{r}_m - \mathbf{r}_u}{\|\mathbf{r}_m - \mathbf{r}_u\|} \right\}^T & 1 \end{bmatrix} \tag{11}$$

The positioning algorithm, being an iterative process, requires adequate initialisation. The choice of the initial state estimate ($\hat{\mathbf{x}}_0$) is fundamental since it can have an impact on the entire procedure. When no a priori information about the state of the receiver is available, in GNSS, a common practice is to initialise the position to the centre of the Earth and set all other state unknowns to zero. In this scenario, the vector $\hat{\mathbf{x}}_0$ becomes an n-component zero vector, where the value of n can vary depending on the positioning algorithm. However, as we will analyse in Section IV, this approach does not always guarantee the convergence of the algorithms.

1. Dilution of precision

The accuracy of state estimation is affected not only by measurement errors but also by the relative spatial arrangement of satellites with respect to the receiver (Morales-Ferre et al., 2020). Furthermore, when dealing with pseudorange rate measurements, the kinematics of satellites also play a crucial role in the achievable performance. The parameters identifying this relationship are known as Dilution of Precision (DOP). There are various types of DOP, each derived from the matrix $\mathbf{G}$, which can be defined as follows:

$$\mathbf{G} = [\mathbf{H^T} \ \mathbf{H}]^{-1} = [g_{D_{i,j}}] \tag{12}$$

depending on the measurement on which the positioning algorithm is based, the matrix $\mathbf{H}$ may have the form of (10) or (11).

A parameter from the DOP family often used in the GNSS literature, and which will serve as a point of comparison for the two algorithms in the following paragraphs, is the Position Dilution of Precision (PDOP), defined as:

$$PDOP = \sqrt{g_{D_{1,1}} + g_{D_{2,2}} + g_{D_{3,3}}} \tag{13}$$

The relationship between PDOP and positioning accuracy is given by the following relation:

$$\sigma_{\mathbf{x_P}} = \sqrt{\sigma_x^2 + \sigma_y^2 + \sigma_z^2} = PDOP \ \sigma_{UERE} \tag{14}$$

Where $\sigma_{\mathbf{x_P}}$ is the standard deviation of the positioning error and σ_{UERE} is the standard deviation of the measurements errror. It can be seen from (14) that the smaller the value of PDOP, the better the performance that can be achieved and the better the geometry of the problem. A final point to consider is that PDOP is dimensionless, and that good satellite geometry is generally reflected in a PDOP value in the range of 2 to 5 (Morales-Ferre et al., 2020).

Similarly to the pseudorange case, we can construct the DOP parameters for Doppler-based positioning. The Doppler Position Dilution of Precision (PDOP_D) is derived from an equation analogous to (13), but the matrix $\mathbf{G}$ in (12) is constructed using the matrix $\mathbf{H_D}$ instead of the matrix $\mathbf{H_P}$. Similarly to the previous case, the DOP relates the error in measurement and the accuracy in positioning, in fact we can obtain the following relationship for the PDOP_D:

$$\sigma_{\mathbf{x_D}} = \sqrt{\sigma_x^2 + \sigma_y^2 + \sigma_z^2} = PDOP_D \; \sigma_{UERRE} \tag{15}$$

Unlike the pseudorange scenario, PDOP_D parameters depend not only on geometry but also on the dynamic trajectories of the satellites (Tan et al., 2019). A first fundamental difference is that they are not dimensionless. By analysing (15), the $PDOP_D$ relates position error expressed in meters to measurement errors that are in meters per second, it can be deduced that $PDOP_D$ must have the dimension of seconds. A further point to consider is the range of values that $PDOP_D$ can generally take. As noted in (Shi et al., 2023), the PDOP_D varies significantly depending on the orbital region considered. In the MEO region, a typical value is about 10^4, while in the LEO region it tends to be about 10^2.

III. METODOLOGY

To evaluate the performance and convergence of the two positioning algorithms in various scenarios, we developed a theoretical framework called "satellite scale-down". This framework allowed us to examine how orbital height and the corresponding speed of the satellites affect both the achievable performance and convergence of the algorithm. As the name of the framework suggests, this involves reducing the altitude of the constellation of satellites considered, while adjusting key parameters such as satellite position and velocity, pseudorange and pseudorange rate measurements to maintain consistency. We explored two main approaches to reducing the orbital height:

Scale-Down method 1: reduce the orbital radii along the LOS vector connecting the receiver to the satellite. This keeps the directions of the steering vector constant in the Jacobian matrix of the ML estimator.

Scale Down method 2: reduce the orbital radii by lowering the satellites along the vector originating from the centre of the Earth and pointing in the direction of the satellites.

Figure 2 visually represents these two methods, with the red dot representing the centre of the Earth and the yellow dot representing the receiver.

The first method seems to support a more realistic deployment of LEO satellites, leading to a denser satellite constellation. This strategy aligns with the dynamics of LEO constellations, which tend to place satellites in close proximity. On the other hand, the second method might better represent a fixed-size constellation that gradually decreases in size. It is worth noting, however, that the latter geometry could pose problems in terms of satellite visibility. As mentioned in the introduction, the footprint of a LEO satellite is significantly smaller than that of a MEO satellite. Therefore, as the orbital radius shrinks, maintaining satellites with this geometry may become unrealistic. For these reasons, in this paper, we have chosen to focus on presenting and analysing the results obtained using the first method.

For each variation in the orbital radius, the satellite's velocity must be adjusted consistently. In our theoretical framework, we considered circular orbits and derived the satellite velocity from the orbital period equation, expressed as follows:

$$T_s \approx 2\pi \sqrt{\frac{r_s^3}{G\,M}} \tag{16}$$

where r_S is the orbital radius of the satellite, M is the mass of the Earth, and G is the universal gravitational constant. From (16) we can derive the expression for the satellite's velocity, v_s, in terms of the orbital radius and two constants, as:

$$v_s \approx \frac{2\pi r_s}{2\pi \sqrt{\frac{r_s^3}{GM}}} = \sqrt{\frac{GM}{r_s}} \tag{17}$$

Finally, starting from (17) and given the velocity of the satellite at its original position, we can determine the velocity of the satellite at the new orbital location:
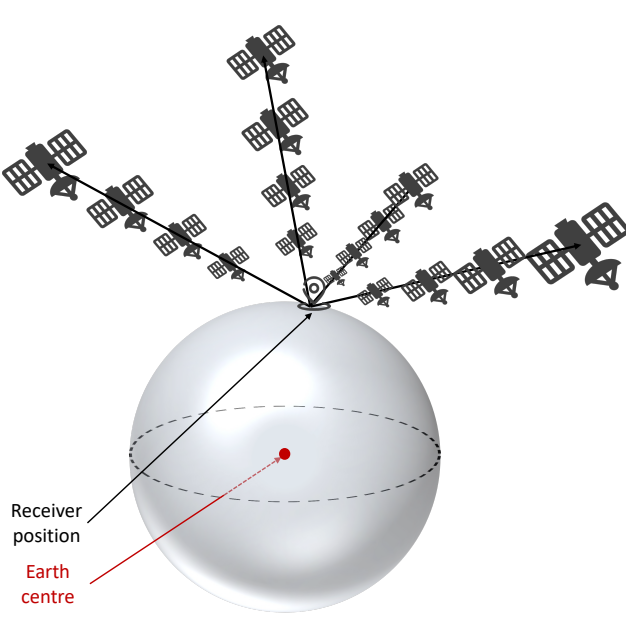
(a) Geometry 1: Lowering satellites along the satellite-receiver LOS.
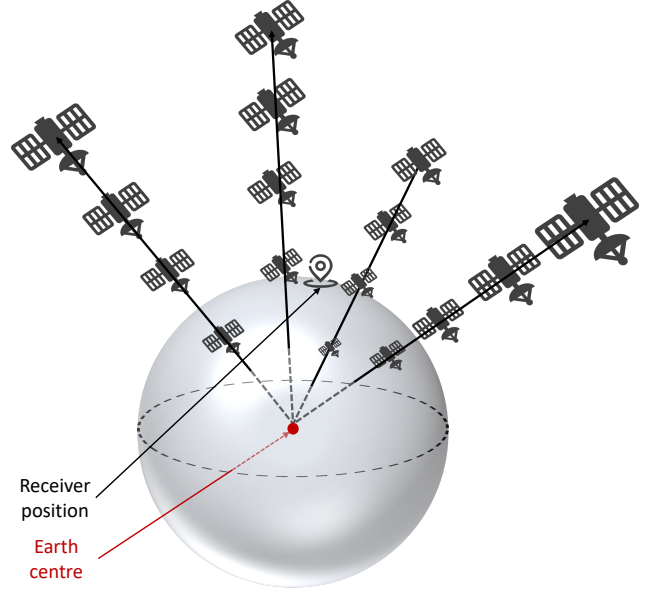
(b) Geometry 2: Lowering satellites along the satellite-centre of the earth direction.

Figure 2: Satellite scale-down geometries.

$$
\begin{cases}
v_{s_1} = \sqrt{\dfrac{GM}{r_{s_1}}} \\
v_{s_2} = \sqrt{\dfrac{GM}{r_{s_2}}}
\end{cases}
\implies
v_{s_2} = v_{s_1}\sqrt{\dfrac{r_{s_1}}{r_{s_2}}}
\tag{18}
$$

Satellite velocity adjustment is not the only parameter to consider in relation to orbital radius. It is also important to fine-tune the pseudorange and pseudorange rate measurements, originally derived from observables. To this end, we generated ideal synthetic measurements based on the ground-truth of the receiver. To make the measurements realistic, we intentionally added a Gaussian noise with zero mean and variance equal to that of the original measurement obtained from the satellite signal at its original position. This choice represents a conservative approach, considering that, as mentioned in Section I, measurements from satellites in the LEO region can be better than those in the MEO region.

IV. RESULTS

In this section, we will focus on analysing the performance of LS algorithms based on pseudorange and Doppler to draw a symbolical view on their capabilities and limitations.

1. Static Receiver with GPS Data

For our first set of results, we evaluated the performance of the algorithm using a static receiver. Data from five satellites of the GPS system were collected using an antenna and a front-end (USRP N210), and then analysed using a software receiver implemented in MATLAB.

For both positioning algorithms, we assume that we have no a priori knowledge of the position of the receiver, so we initialise the algorithm with $\hat{x}_0 = 0$. In addition, given the nature of the receiver, we have neglected the user velocity considering it equal to zero. This simplification helps to reduce the information representing the state of the receiver.

The spatial distribution of the satellites used for the fix is shown in the sky plot in Figure 3. This satellite geometry is reflected in a mean values of the PDOP and PDOP$_D$ parameters on the epochs, which are 3.28 and 20975.38 s respectively. It is worth noting the large discrepancy between these two values, and also that the order of magnitude of the PDOP$_D$ (10^4) is in line with what is reported in (Shi et al., 2023). Nevertheless, a PDOP value below 5 indicates the presence of a good satellites distribution.

Figure 4 qualitatively illustrates the differences in performance between the two algorithms. The figure illustrates the distribution of position estimates along with their respective 95 % covariance error ellipses for both algorithms. Dark blue represents the
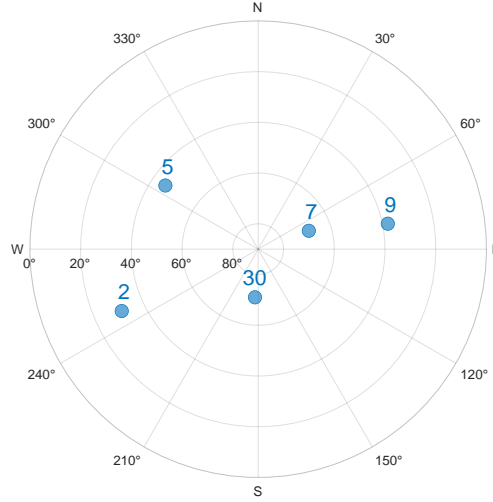
Figure 3: Skyplot of simulated satellites

Doppler positioning data, while light blue corresponds to Pseudorange positioning data. Triangles denote the mean values of the position estimate distributions. The midpoint of the Pseudorange position estimates is located at coordinates Latitude, longitude, and altitude (LLA) $\bar{\mathbf{r}}_{\mathbf{P}} = [45.0653148390768; 7.65892248028871; 321.106505556963]$. This point is important because it is taken as a reference for all subsequent error analyses. From Figure 4, can be observed that the covariance ellipse associated with Doppler positioning encloses a significantly larger area compared to the one associated with Pseudorange positioning. The latter is more compact around the receiver's position, suggesting better precision and accuracy in Pseudorange-based positioning.
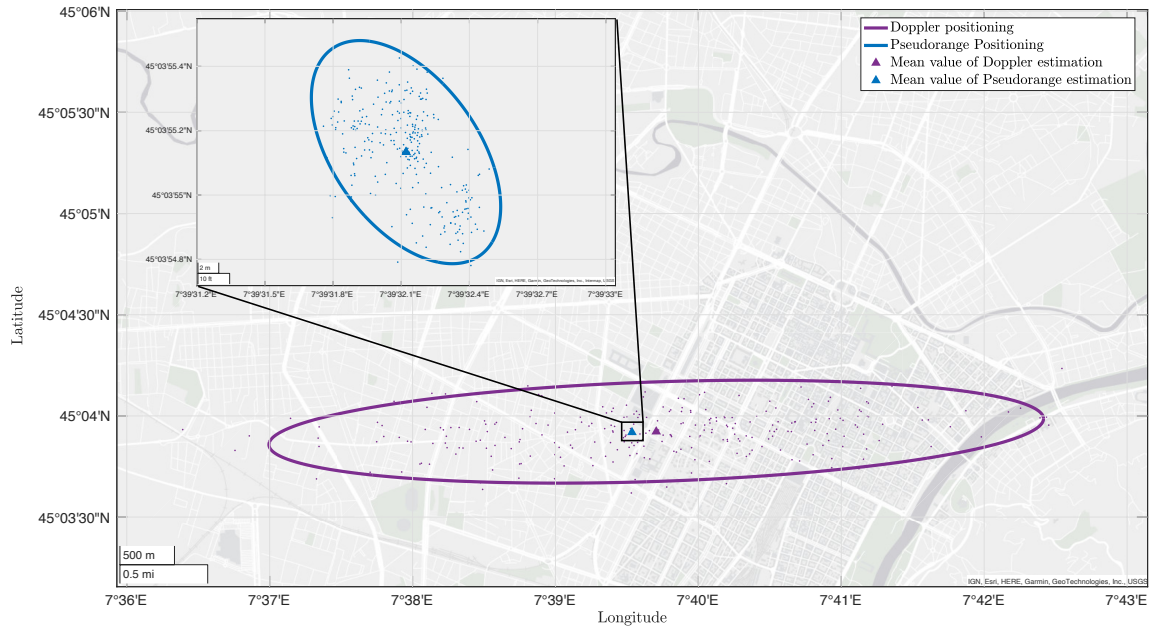

Figure 4: Comparison of 95 % covariance error ellipse for both pseudorange and Doppler-based positioning.

Moving on to a more quantitative analysis, Figure 5 shows the error curves for position in 3D, horizontal and vertical relative to $\bar{\mathbf{r}}_{\mathbf{P}}$ in East, North, Up (ENU) reference frame. Moreover, Tables 1 and 2 summarise the mean, maximum and minimum error values as well as the Root Mean Square (RMS) for both algorithms. We observe that the pseudorange algorithm has an error that oscillates between 0 and $32\,\mathrm{m}$, while the Doppler algorithm has an error with peaks that reach up to $4\,\mathrm{km}$. It is interesting to note the trend of the vertical error compared to the horizontal one. While with the pseudorange algorithm, as expected, the vertical error is almost always greater than the horizontal one, with the Doppler algorithm it is instead the opposite. This trend

is well known in the literature and is attributed to the conical geometry which favours the vertical direction over the horizontal (Van Graas, 2023).

In terms of positioning accuracy and precision, there is a significant difference between the two considered algorithms when using GPS satellites in the MEO region. Classical positioning based on pseudorange measurements outperforms the Doppler-based approach. The sub-optimal performance of the latter in the MEO region can be attributed to the lower speeds of the satellites compared to what they could have in the LEO region (approximately $3.9\,\text{km/s}$), resulting in more moderate variations in the Doppler measurements. The use of satellites in the LEO region, which experience greater Doppler shift variations due to their speed, can lead to improved positioning performance.
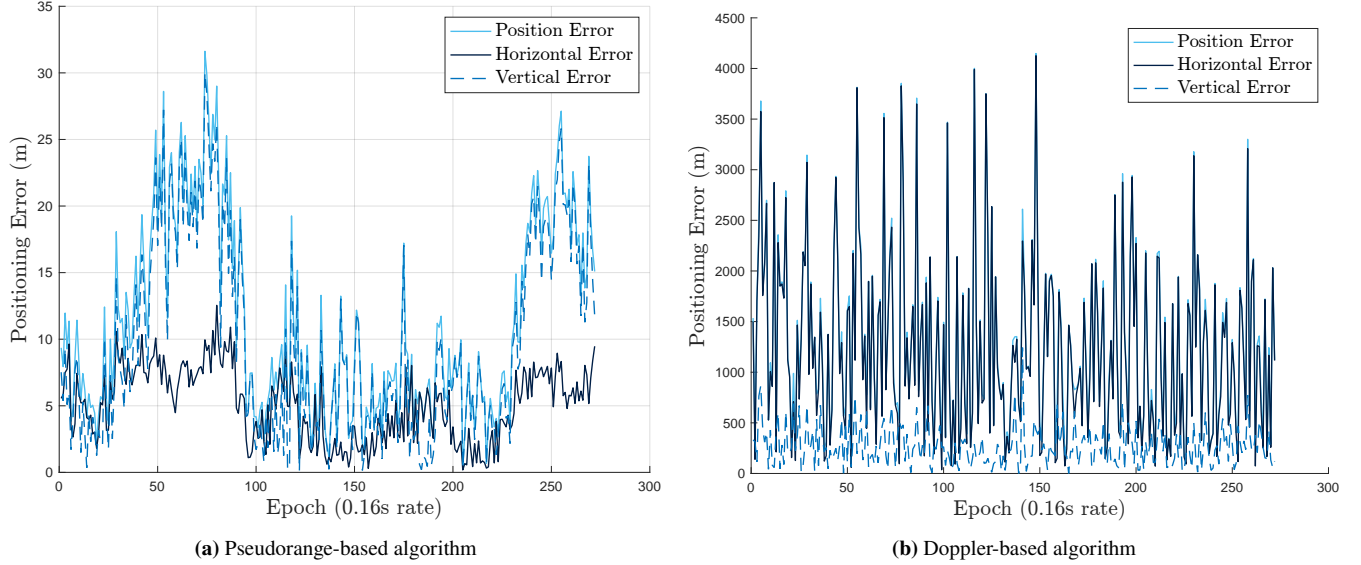

(a) Pseudorange-based algorithm

(b) Doppler-based algorithm

Figure 5: Position, horizontal and vertical error.

Table 1: Mean, Maximum, Minimum and RMS values of 3D position, horizontal and vertical errors for pseudorange-based positioning in the ENU reference frame.

	mean value	max value	min value	RMS
Position error (m)	11.343	31.620	0.378	13.435
Horizontal error (m)	5.071	12.542	0.118	5.758
Vertical error (m)	9.707	30.0128	0.102	12.138

Table 2: Mean, Maximum, Minimum and RMS values of 3D position, horizontal and vertical errors for Doppler-based positioning in the ENU reference frame.

	mean value	max value	min value	RMS
Position error (km)	1.278	4.147	0.085	1.540
Horizontal error (km)	1.218	4.125	0.036	1.504
Vertical error (km)	0.268	1.243	0.00089	0.3320

2. Results varying orbital radius

Considering the unsatisfactory performance of Doppler positioning in the MEO region, we explored the possibility of achieving better accuracy with lower orbits. For this purpose, we utilised the theoretical "satellite scale-down" framework outlined in Section III. We initially confirmed the convergence of the LS algorithm through Monte Carlo simulations. Subsequently,

we investigated the performance attainable with satellites at a lower altitude than GPS. To ensure a fair comparison with the previously obtained results, we choose to simulate the same scenario using the same satellites.

a) Sensitivity to initial position estimate

The positioning algorithm based on the LS estimator requires proper initialisation for convergence. The common practice of initialising the algorithm by placing the initial estimate at the centre of the Earth does not always lead to convergence, especially in LEO regions (Shi et al., 2023; Van Uytsel et al., 2023). With this in mind, we performed Monte Carlo simulations to investigate how the convergence of the algorithm is affected by varying the distance between the initial position estimate and the receiver as the satellite's orbit decreases.

In this simulation we considered a set of 100 orbital radii, 60 in the LEO region and 40 in the MEO region, up to the orbital altitude of the GPS satellites ($20200\,\text{km}$). In addition, we considered a set of 111 distances: 39 in the range $0 - 950\,\text{km}$ with a step of $25\,\text{km}$, 71 in the range $1000 - 6300\,\text{km}$ with a step of $75\,\text{km}$, and a final distance of about $6367\,\text{km}$, corresponding to the distance of the receiver from the centre of the Earth. These distances are used to indicate how far from the receiver the initialisation estimate ($\hat{\mathbf{x}}_0$) is set. We denote these distances mathematically with the parameter δ_r, defined as:

$$\delta_r = \|\bar{\mathbf{r}}_{\mathbf{P}} - \hat{\mathbf{r}}_0\| \tag{19}$$

where $\bar{\mathbf{r}}_{\mathbf{P}}$ 3-component vector representing the position of the mean value of the pseudorange estimate while $\hat{\mathbf{r}}_0$ is a 3-component vector representing position of $\hat{\mathbf{x}}_0$. Each initialisation state $\hat{\mathbf{x}}_0$ takes the form of:

$$\hat{\mathbf{x}}_0 = [\hat{\mathbf{r}}_0 \ 0]^T \tag{20}$$

where 0 represents the initial estimate for the clock bias or clock drift, depending on the positioning algorithm considered. To assess the validity of a distance, we generate a set of 2500 possible initialisation states ($\hat{\mathbf{x}}_0$) randomly distributed on the surface of a sphere centred at $\bar{\mathbf{r}}_{\mathbf{P}}$ and of radius δ_r. The random distribution guarantees coverage in all directions.

A tested distance is considered valid only if all 2500 initial positions lead to convergence of the algorithm. Convergence is defined by an average convergence norm over epochs of less than 10^{-6} and an average horizontal error over epochs of less than $10\,\text{km}$ with respect to $\bar{\mathbf{r}}_{\mathbf{P}}$. If these conditions are not met as the orbital radius decreases, a smaller distance from the receiver is considered for the same orbital radius.

Figure 6 compares the sensitivity of the positioning algorithm based on the LS estimator at the time of initialisation, using both pseudorange and pseudorange rate measurements. Figure 6a illustrates the performance in the LEO region, while Figure 6b illustrates the performance in the MEO region.

The graph shows, for each orbital radius considered, the first distance (δ_r) that leads to convergence of the algorithm. The performance of the pseudorange-based algorithm is represented by the orange curve, while the Doppler-based algorithm is represented in blue. The two vertically dashed black lines indicate the altitude of the GPS (20200 km) and IRIDIUM (781 km) constellations.

The trend observed in both curves shows that as the orbital radius decreases, both algorithms have difficulties to set the initial position estimates at the centre of the Earth. Consequently, they require greater proximity to the receiver in order to converge. Moreover, it can be seen that the LS positioning algorithm based on pseudorange measurements seems to be more robust in terms of algorithm convergence. In fact, a flat region can be observed in the curve of the pseudorange algorithm, indicating that despite the reduction in the orbital radius of the satellites, the algorithm still manages to converge without the need for a priori knowledge of the receiver. The discrepancy between the two algorithms can be attributed to the fact that the Doppler algorithm depends not only on the position of the satellites but also on the kinematics.

The simulation also reveals that convergence problems are not confined to the LEO region, but extend to the MEO region as well. In particular, the pseudorange rate algorithm encounters the need to adjust the position of $\hat{\mathbf{x}}_0$ closer to the receiver at an altitude of about 19733 km. In contrast, the algorithm based on pseudorange measurements shows a convergence capability up to an altitude of 13200 km.

To complement the visual insights, Table 3 reports some values extracted from the graphs in Figure 6.
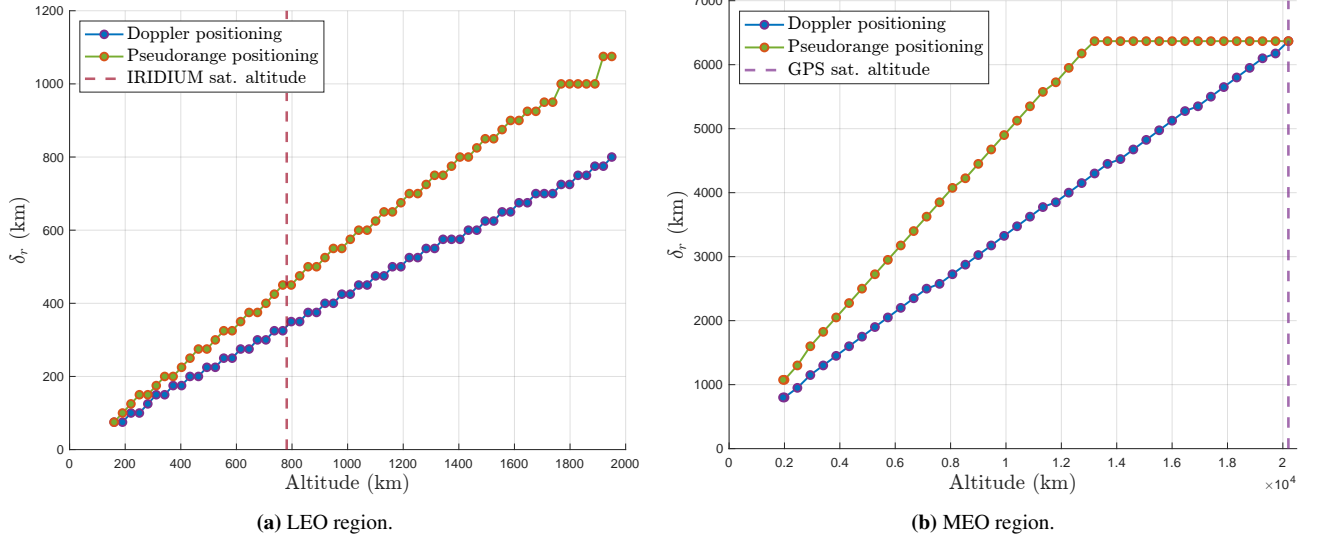
(a) LEO region.

(b) MEO region.

Figure 6: Comparison of initial position estimate on Pseudorange and Doppler-based LS algorithm to the change in orbital altitude.

Table 3: Selected values from Figure 6 illustrating the convergence behaviour of the Pseudorange and Doppler-based algorithms at different orbital altitudes.

	Orbital Altitude (km)	$\delta_{\mathbf{r}}$ (km)	
		Pseudorange	Doppler
LEO Region	160	75	75
	615	350	275
	1070	600	450
	1525	850	625
	1950	1075	800
MEO Region	2000	1075	800
	6667	3400	2350
	11333	5575	3775
	16000	6367	5125
	20200	6367	6367

b) Algorithm performance

To investigate the performance of the LS positioning algorithm, especially at lower orbital altitudes than GPS, we performed Monte Carlo simulations using the same setup used in Section IV.2 a). In this evaluation, the initialisation point of the algorithm was placed at a distance of 75 km from the reference point $\bar{\mathbf{r}}_{\mathbf{P}}$. This specific distance was chosen on the basis of the results obtained in the previous section, where it was found that all the orbital radii under test led to convergence at this distance.

Figure 7 shows the PDOP parameter trend for both positioning algorithms, while Table 4 presents selected values from the corresponding graph. The PDOP trend for the pseudorange-based positioning algorithm remains relatively constant, maintaining an average value of approximately 3.2832. This trend is consistent with the geometry resulting from the lowering of the satellites, which keeps the direction of the steering vectors constant. On the other hand, the PDOP_D for the shows shows a decreasing trend as the orbital radii decrease. It assumes values of the order of 10^4 in the MEO region and reaches values of the order of the order of 10^2 in the LEO region.

In terms of positioning errors relative to the reference point $\bar{\mathbf{r}}_{\mathbf{P}}$, Figures 8a and 9 show the trend in horizontal errors, while Figure 10 shows the trend in vertical errors. Table 5 gives a summary of some selected values. Consistent with the trend observed
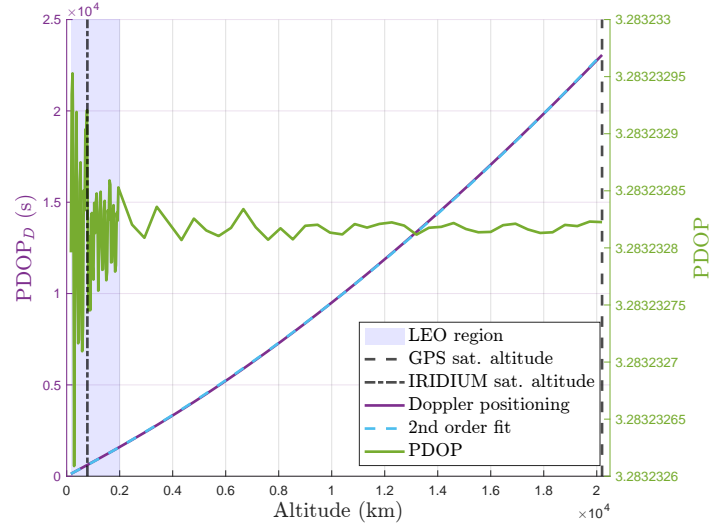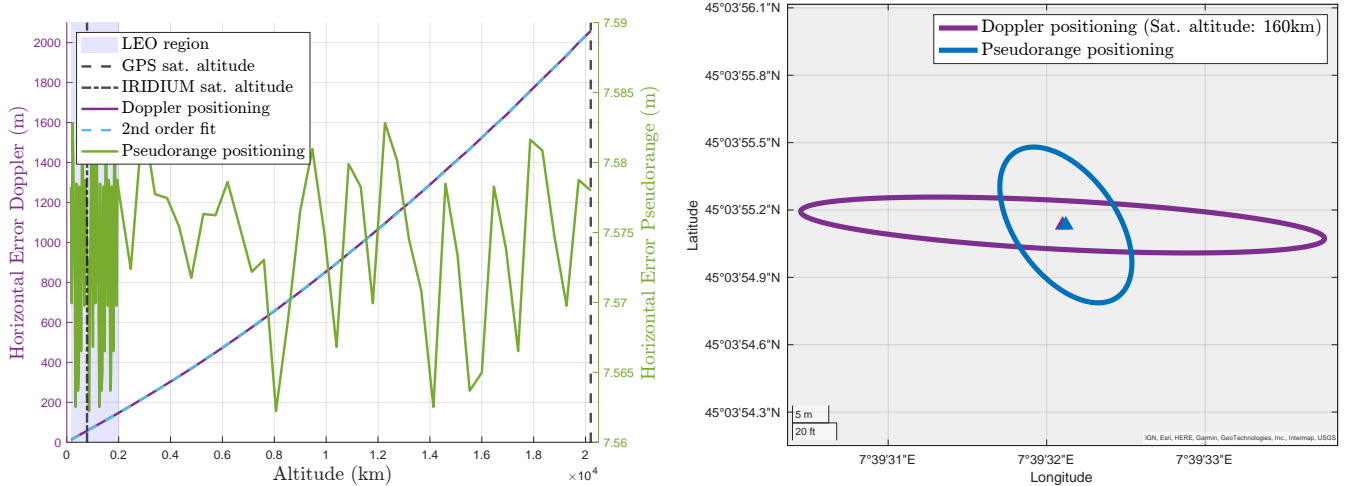
Figure 7: Comparison of PDOP for Pseudorange and Doppler-based LS algorithm to the change in orbital altitude.

in Figure 7, the horizontal error for the pseudorange-based algorithm remains relatively stable, showing minimal variation as orbital altitude decreases. In contrast, the trend for the Doppler-based algorithm shows a marked improvement that is reflected on an average horizontal error of approximately 12 m for an orbital altitude of 160 km. This is a relevant gain considering the initial error observed in 5b of over 1 km. To highlight the improvement achieved by the Doppler algorithm, Figure 8b shows a comparison between the 95 % covariance error ellipse associated with the pseudorange algorithm with the satellites in their original position, and the covariance ellipse of the Doppler algorithm with the satellites at an altitude of 160 km. As expected from the numerical values, in this scenario the ellipse associated with the Doppler algorithm, while retaining its original shape due to geometric considerations, has narrowed considerably around $\bar{\mathbf{r}}_{\mathbf{p}}$.

(a) Comparison of Horizontal error for Pseudorange and Doppler-based LS algorithm to the change in orbital altitude.

(b) Comparison of the 95 % covariance error ellipse: pseudorange algorithm (with GPS satellites) and the Doppler algorithm (satellite altitude: 160 km).

Figure 8: Horizontal error

Figure 9 further examines the evolution of the horizontal errors by distinguishing between the LEO and MEO regions, along with the associated uncertainties for each data point. Observing the scale of values on the y-axis, it can be appreciated that from the MEO to the LEO region there is a decrease in the level of uncertainty, which is reflected in an improvement in positioning performance.

On the other hand, the trend of the vertical mean error, shown in Figure 10, underlines once again the smaller error in the vertical direction than in the horizontal, due to the geometrical consideration on conical surface.

Table 4: Selected values from Figure 7 illustrating the Position DOP behaviour of the Pseudorange and Doppler-based algorithms at different orbital altitudes.

| | Orbital Altitude (km) | Position DOP | |
		Pseudorange	Doppler
LEO Region	160	3.2832	129.5031 s
	615	3.2832	488.8675 s
	1070	3.2832	849.4508 s
	1525	3.2832	1.2143e+03 s
	1950	3.2832	1.5640e+03 s
MEO Region	2000	3.2832	1.6016e+03 s
	6667	3.2832	5.8896e+03 s
	11333	3.2832	1.1071e+04 s
	16000	3.2832	1.7057e+04 s
	20200	3.2832	2.3062e+04 s

V. CONCLUSIONS

This paper compares the LS positioning algorithm based on pseudorange measurements and Doppler measurements in different scenarios at different satellite altitudes exploiting the theoretical framework named "scale-down". The results show that due to the low variability of Doppler measurements, the performance of the Doppler algorithm is significantly worse than the traditional pseudorange-based algorithm in the MEO regions. On the other hand, in the LEO region, where the velocity of the satellites increase, and so does the variability of the Doppler measurement, a significant gain in performance is observed, with an average horizontal error of about 12 m being obtained at the boundaries of the LEO region. However, the use of the LEO region presents a challenge in terms of algorithm convergence. Initialising the algorithm with no prior information is no longer feasible as the algorithm does not converge. This requires a trade-off between the achievable performance and the available receiver information that guarantees the convergence of the algorithm. Future work should further investigate the performance analysis with different geometries and understand the nature of the convergence. By broadening the scope of the simulations and analysing a wider set of scenarios, a theoretical trend could be extracted that would provide a deeper understanding of the convergence of the algorithm and how it can be ensured.
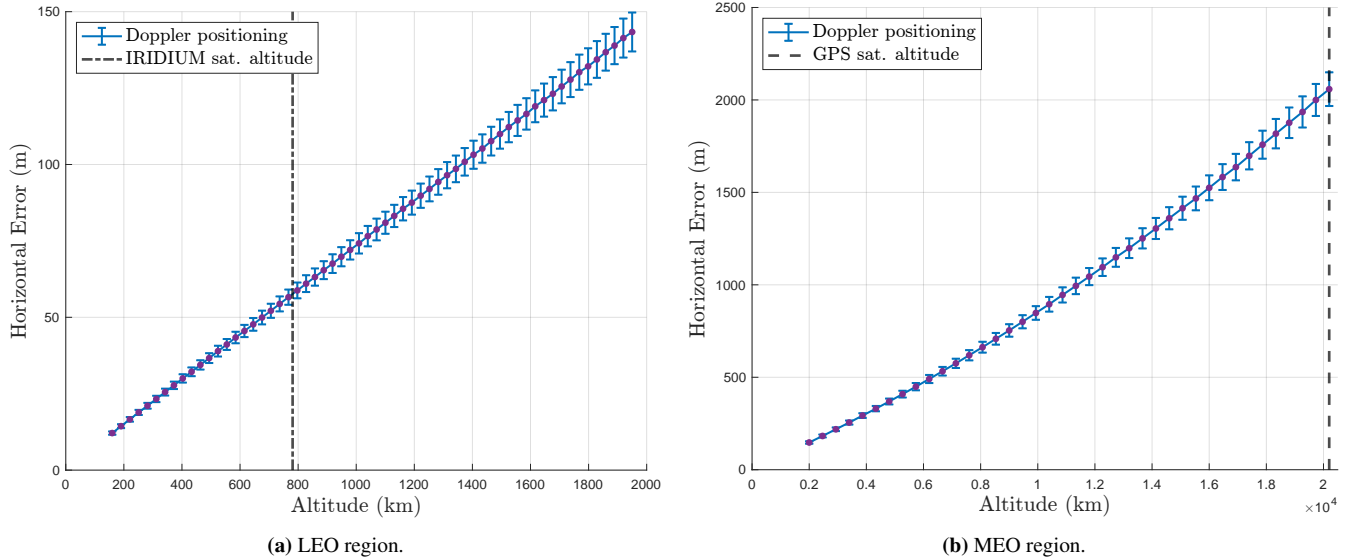

(a) LEO region.

(b) MEO region.

Figure 9: Comparison of Horizontal error for Doppler-based LS algorithm to the change in orbital altitude with the uncertainties associated to each points.
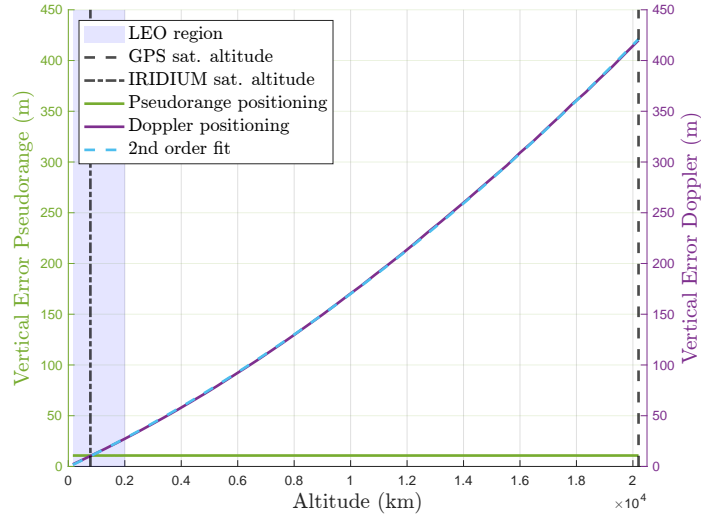
Figure 10: Comparison of Vertical Error for Doppler-based LS algorithm to the change in orbital altitude.

Table 5: Selected values from Figure 8a and Figure 10 illustrating the horizontal and vertical error of the Pseudorange and Doppler-based algorithms at different orbital altitudes.

	Orbital Altitude (km)	Horizontal Error (m)		Vertical Error (m)	
		Pseudorange	Doppler	Pseudorange	Doppler
LEO Region	160	7.5783	12.1191	10.7643	2.1190
	615	7.5809	45.5232	10.7377	8.1132
	1070	7.5783	78.7314	10.7463	14.2354
	1525	7.5809	112.2349	10.7573	20.5141
	1950	7.5788	143.3540	10.7720	26.5747
MEO Region	2000	7.5780	147.2606	10.7681	27.2654
	6667	7.5754	532.6842	10.7377	104.2097
	11333	7.5783	994.2596	10.7463	198.8981
	16000	7.5650	1.5247e+03	10.7570	309.1284
	20200	7.5780	2.0582e+03	10.7681	419.9218

REFERENCES

Bahrami, M. and Ziebart, M. (2010). Instantaneous Doppler-aided RTK positioning with single frequency receivers. In *IEEE/ION Position, Location and Navigation Symposium*, pages 70–78.

Braasch, M. and van Dierendonck, A. (1999). GPS receiver architectures and measurements. *Proceedings of the IEEE*, 87(1):48–64.

Grewal, M. S., Weill, L. R., and Andrews, A. P. (2001). *Global positioning systems, inertial navigation, and Integration*. Wiley.

Kassas, Z. (2021). *Navigation from Low-Earth Orbit (Part 2)* , volume 2. Wiley.

Khalife, J. J. and Kassas, Z. M. (2019). Receiver design for Doppler positioning with LEO satellites. In *ICASSP 2019 - 2019*

IEEE International Conference on Acoustics, Speech and Signal Processing (ICASSP), pages 5506–5510.

Kozhaya, S. E. and Kassas, Z. M. (2023). Positioning with Starlink LEO satellites: A blind Doppler spectral approach. In *2023 IEEE 97th Vehicular Technology Conference (VTC2023-Spring)*, pages 1–5.

Lethinen, A. (2002). Doppler positioning with GPS. Master's thesis, Tampere University of Technology (TUT), Tampere.

Morales-Ferre, R., Lohan, E. S., Falco, G., and Falletti, E. (2020). GDOP-based analysis of suitability of LEO constellations for future satellite-based positioning. In *2020 IEEE International Conference on Wireless for Space and Extreme Environments (WiSEE)*, pages 147–152.

Psiaki, M. L. (2021). Navigation using carrier doppler shift from a LEO constellation: TRANSIT on steroids. *NAVIGATION: Journal of the Institute of Navigation*, 68(3):621–641.

Reid, T. G., Neish, A. M., Walter, T., and Enge, P. K. (2018). Broadband LEO constellations for navigation. *NAVIGATION*, 65(2):205–220.

Shi, C., Yulu, Z., and Li, Z. (2023). Revisiting doppler positioning performance with LEO satellites. volume 27.

Tan, Z., Qin, H., Cong, L., and Zhao, C. (2019). New method for positioning using IRIDIUM satellite signals of opportunity. *IEEE Access*, 7:83412–83423.

Van Graas, F. (2023). Doppler processing for satellite navigation. In *2023 IEEE/ION Position, Location and Navigation Symposium (PLANS)*, pages 365–371.

Van Uytsel, W., Janssen, T., Halili, R., and Weyn, M. (2023). Exploring positioning through pseudoranges using low earth orbit satellites. In Barolli, L., editor, *Advances on P2P, Parallel, Grid, Cloud and Internet Computing*, pages 278–287, Cham. Springer International Publishing.